

SCIENTIFIC REPORTS



OPEN

Characterization of coumarin-6 polycrystalline films growth from vacuum deposition at various substrate temperatures

Ko-Lun Chen, Hui-Ting Liu, Jang-Hung Yu, Yung-Hsiang Tung, Yun-Syuan Chou, Chun-Chuen Yang, Jyh-Shyang Wang, Ji-Lin Shen & Kuan-Cheng Chiu

Coumarin-6 polycrystalline films were fabricated from vacuum deposition at various substrate temperatures T_{sub} from 106 to 178 °C with a fixed source temperature of 185 °C. Because of its slenderer and more asymmetric structure, the adhered coumarin-6 molecule on top of the growing interface encounters a larger steric energetic barrier of 0.92 eV as estimated from the Arrhenius plot of growth rate versus $1/T_{sub}$. From top-view SEM pictures, the as-deposited coumarin-6 thin films exhibit a twisted pattern and a kinematic roughness for $T_{sub} < 150$ °C; while clear facets emerge for $T_{sub} \geq 150$ °C due to the increase of surface diffusion energy of the adhered molecules. From XRD analysis, besides the confirmation of the triclinic structure two anomalous peaks observed at $2\theta \sim 9.007^\circ$ and 7.260° are explained due to the co-existence of N- and S-coumarin-6-isomers within the crystalline grains. Furthermore, for coumarin-6 polycrystalline films deposited at $T_{sub} = 150$ °C with high crystallinity of the constituent grains, the bandgap determined from optical transmission is around 2.392 eV; and from photoluminescence spectra, the fitted four emission components are assigned to the Frenkel and charge transfer excitons recombination with participation of molecular vibrational states.

The small organic molecule of 3-(2-benzothiazolyl)-7-(diethylamino)coumarin ($C_{20}H_{18}N_2O_2S$, named as coumarin-6 or coumarin-540)¹ has been known and utilized as one of the fluorescent dyes for staining organelles or materials used in medicine^{2,3}, and for high-gain medium in tunable and amplifier lasers⁴⁻⁶. Moreover, after being successfully introduced as an efficient dopant in organic light emitting diodes⁷, coumarin-6 has also attracted much interest in optoelectronic applications⁸⁻¹³. Coumarin-6 is a molecular chromophore with high quantum efficiency. While dissolved in various solvents, the absorption maximum ranged from 2.713 eV (in methanol or ethanol) to 2.912 eV (in n-hexane) and photoluminescence (PL) with peak emission maximum from 2.460 eV (in methanol) to 2.702 eV (in n-hexane) were reported⁵. As crystallized from supersaturated solutions, coumarin-6 tiny single crystal has a triclinic structure with lattice parameters $a = 8.962$ Å, $b = 11.136$ Å, $c = 8.922$ Å, $\alpha = 95.14^\circ$, $\beta = 104.50^\circ$, and $\gamma = 86.74^\circ$ ^{1,14}. Coumarin-6 molecular crystal possesses a relatively high melting point around 220 °C, a high stability of surface morphology, and an efficient light emission, and hence can be considered as an important organic material for optoelectronic devices. However, for acting as a dye or dopant in optoelectronic devices, only the molecular characters of coumarin-6 are focused. While in organic multilayer optoelectronic devices, a systematic study on the fabrication and characterization of coumarin-6 polycrystalline or amorphous thin films is prerequisite.

Vacuum deposition (*i.e.*, deposition by thermal sublimation in vacuum) is one of the most common techniques adopted for depositing small organic molecular thin films if these molecules can be sublimed at an appropriate source temperature (T_{sou}) without decomposition^{7,15-17}. To obtain a significant growth rate, the vapor pressure from source powder governed by T_{sou} has to be high enough. The T_{sou} -dependence of vapor pressure can be determined from the rate of mass loss per unit area by using a conventional thermogravimetric analysis (TGA)^{18,19}. Besides, the substrate temperature (T_{sub}) governs the surface kinetics of the adhered molecules, including adhesion, surface diffusion, and re-evaporation of the incoming molecules onto the substrate surface as

Department of Physics and Center for Nanotechnology, Chung Yuan Christian University, Chungli District, Taoyuan City, 32023, Taiwan. Correspondence and requests for materials should be addressed to K.-C.C. (email: kcchiu@cycu.edu.tw)

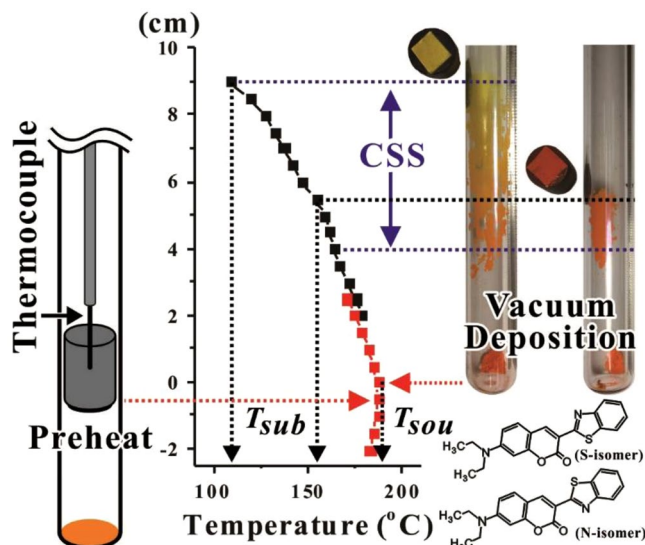


Figure 1. Growth ampoule under pre-heat process and after vacuum deposition with CSS region are schematically demonstrated. Two coumarin-6 films (on ITO substrate with graphite susceptor) deposited with different T_{sub} are illustrated. The S- and N-isomers by turning the benzothiazolyl moiety upto 180° are depicted.

well as the growing interface. The difference between T_{sou} and T_{sub} corresponds to the degree of supersaturation which affects the nucleation and subsequent growth^{20–26}. The proper values of T_{sub} corresponding to a fixed T_{sou} can be experimentally determined from the concept of constitutional supersaturation (CSS), and the effects of T_{sub} on the size, orientation, and crystallinity of the constituent grains and on the growth rate of various small organic molecular polycrystalline films were reported^{21–25}.

Within a coumarin-6 molecular crystal, as demonstrated in Fig. 1, the coumarin moiety is nearly coplanar with the benzothiazolyl moiety (*i.e.*, the pyrone ring in the essentially planar structure of coumarin moiety makes a small angle of 2.30° with the thiazolyl ring and 3.29° with the benzene ring in the benzothiazolyl moiety, respectively)¹. However, in coumarin-6 crystalline grains, two conformational isomers (namely, S-isomer and N-isomer) should be distinguished by turning the benzothiazolyl moiety upto 180° such that the relative position of S or N atom in the benzothiazolyl moiety with respect to the O atom in the coumarin moiety is different. So far, there is no report in literature on these two isomers. Thus, the effects from these isomers on the properties of the as-grown coumarin-6 molecular solid films remain to be clarified.

In this work, coumarin-6 polycrystalline films on indium-tin-oxide (ITO) substrate were grown from vacuum deposition at various T_{sub} with a fixed T_{sou} . The growth behavior of coumarin-6 polycrystalline films is studied in terms of an Arrhenius plot of growth rate versus $1/T_{sub}$. The corresponding steric energetic barrier E_A on the formation of coumarin-6 molecular solid films is discussed and compared with other small organic molecules with different space symmetries. In addition, the morphological, structural, and optical properties of the as-deposited coumarin-6 polycrystalline films with respect to T_{sub} are also systematically investigated with respect to the S- and N-isomers. This work, though of technological importance to the fabrication of coumarin-6 thin films for applications in organic multilayer devices, is also expected to clarify some fundamental problems of crystallization mechanisms, weak intermolecular interactions, and surface kinematic effects for the production of organic molecular solids.

Results and Discussion

Determining the deposition conditions from TGA and CSS. The temperature (T)-dependence of equilibrium vapor pressure from the source powder plays an important role during the vacuum deposition process^{20–25}. However, the data of vapor pressure over a wide enough T range for some small organic molecules are often difficult to obtain, and based on our literature survey the relevant information for coumarin-6 is not available. Thus, by using a conventional TGA, a method relating the vapor pressure with the rate of mass loss per unit area was adopted^{18,19}. The inset in Fig. 2 demonstrates the TGA curve for coumarin-6 with a heating rate of $dT/dt = 10^\circ\text{C}/\text{min}$, and Fig. 2 represents the rate of mass loss percentage, $-d(M(t)/M_0)/dt$, versus $1000/T$ (here T is in Kelvin scale), where $M(t)$ is the mass at time t and M_0 is the initial mass of the sample. The data in Fig. 2 could be fitted by a function of $A \times \exp(-H_F/kT) + B$, where H_F is associated with the enthalpy of fusion, k is the Boltzmann constant, and A and B are constants^{16–19}. For $T < T_0$, $M(t)$ remained nearly unchanged as depicted in the inset, thus the very low and rather noisy values of $-d(M(t)/M_0)/dt$ were represented by a background B value. At $T = T_0$ ($\cong 175^\circ\text{C}$), the deviation of the fitted curve from the background B level indicated a threshold of sublimation loss. For $T \gg T_1$, the slope of the fitted straight line was associated with H_F ($\cong 1.08$ eV), and the intercept point of the straight line with the background B was related to the melting point ($T_1 \cong 224^\circ\text{C}$). To obtain a reasonable sublimation rate for thin film deposition, T_{sou} could be empirically selected around T_0 . In this work, $T_{sou} = 185 \pm 2^\circ\text{C}$ was chosen, then the side wall deposition corresponding to a CSS zone is demonstrated in Fig. 1.

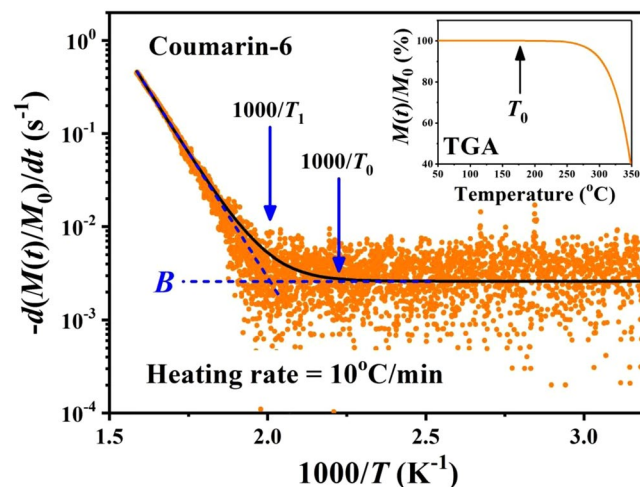


Figure 2. The rate of mass loss percentage, $-d(M(t)/M_0)/dt$, versus $1000/T$ for coumarin-6 source powder. T_0 ($\cong 175^\circ\text{C}$) indicates a threshold of sublimation loss, and T_1 ($\cong 224^\circ\text{C}$) is associated with the melting point for coumarin-6 powder. The inset demonstrates the TGA curve with a heating rate of $dT/dt = 10^\circ\text{C}/\text{min}$.

The CSS zone is a region where the actual vapor pressure exceeds the equilibrium vapor pressure such that the degree of supersaturation is large enough for nucleation and subsequent growth^{21–25}. Based on the spreading of CSS zone, T_{sub} was varied from 106 to 178 °C, and the deposition period $\tau = 51 \pm 1$ min was chosen.

Usually, the growth modes in vacuum deposition can be categorized into mass-transport controlled regime and surface-kinetics controlled regime^{20,26}. In this work with a high enough T_{sou} ($> T_0 \cong 175^\circ\text{C}$), the free space between source and substrate is nearly occupied with the convection of vaporized molecules with vapor pressure determined by T_{sou} . Only near the substrate side a very thin diffusion boundary layer exists. As a CSS region is observed on sidewall near substrate side, the growth behavior on top of the substrate is dominated by surface-kinetics controlled regime. Consequently, the properties of the as-deposited molecular solid films are sensitively dependent on T_{sub} .

Surface morphology of coumarin-6 films fabricated at various T_{sub} . Figures 3 and 4 show the top- and side-view SEM pictures of coumarin-6 polycrystalline films deposited at various T_{sub} , respectively. For a substrate located within the CSS region, the flux of incoming vaporized molecules is larger than the flux from re-evaporation, thus the net growth behavior is dominated by the surface-kinetics controlled regime²⁶. Hence, both the adhesive probability of the incident molecules and the surface diffusion energy of the adhered molecules on the substrate as well as on the growing interface are increased with increasing T_{sub} . From Figs. 3 and 4, for the lowest T_{sub} of 106 °C, the adhesive probability of the incoming coumarin-6 molecule on the substrate was not high enough, thus the coverage of the coumarin-6 thin film on the ITO substrate was incomplete. Until $T_{sub} \geq 125^\circ\text{C}$, the coverage become complete, and from the side-view SEM pictures the average thin film thickness L_D was estimated. Furthermore, from the top-view SEM pictures as shown in Fig. 3, for $125^\circ\text{C} \leq T_{sub} < 150^\circ\text{C}$, the adhered coumarin-6 molecules on the interface do not have enough surface kinetic energy to re-arrange their relative conformation and to diffuse to the appropriate growth sites, thus the as-deposited coumarin-6 thin films exhibited a twisted pattern and a slightly kinematic roughness. Until $T_{sub} \geq 150^\circ\text{C}$, clear facets corresponding to coumarin-6 crystalline grains emerged.

Growth behavior of coumarin-6 thin films. As shown in Fig. 4, the coverage of coumarin-6 solid films on ITO substrate become complete for $T_{sub} \geq 125^\circ\text{C}$, and from the side-view SEM pictures the average thin film thickness L_D was estimated. Together with the deposition period τ , the growth rate of coumarin-6 polycrystalline films was obtained. The Arrhenius plot of growth rate versus $1000/T_{sub}$ (here T_{sub} is in Kelvin temperature scale) is demonstrated in Fig. 5. For an organic molecular crystal growth from vapor phase, the adhered molecules have to overcome a steric energetic barrier E_A in order to occupy the appropriate location (with more nearest neighbors) and the correct orientation (to maximize the intermolecular interactions)²⁶. The corresponding E_A for coumarin-6 polycrystalline films evaluated from the Arrhenius plot was about 0.92 ± 0.06 eV. Together with our previous works for C_{60} , Alq3, rubrene and CuPc^{21–24}, the related parameters for these small organic molecular solid films deposited within the CSS region are summarized. Due to its slenderer and more asymmetric structure accompanied by a larger permanent dipole, the coumarin-6 molecules were expected to encounter a higher steric hindrance to occupy the appropriate location and correct orientation, and hence possessed a larger E_A .

XRD analysis of coumarin-6 films fabricated at various T_{sub} . Figure 6 illustrates the XRD patterns for (a) the coumarin-6 polycrystalline films on top of ITO substrates in a normalized and linear scale and (b) the coumarin-6 powders taken from the as-deposited films in a logarithmic scale, separately. The Miller indices of the main peaks were assigned based on Crystallography Open Database for COD ID 2003249¹. As depicted in Fig. 6(a), a protruding peak at $2\theta = 8.039 \pm 0.009^\circ$ corresponding to the (010) peak was observed for all

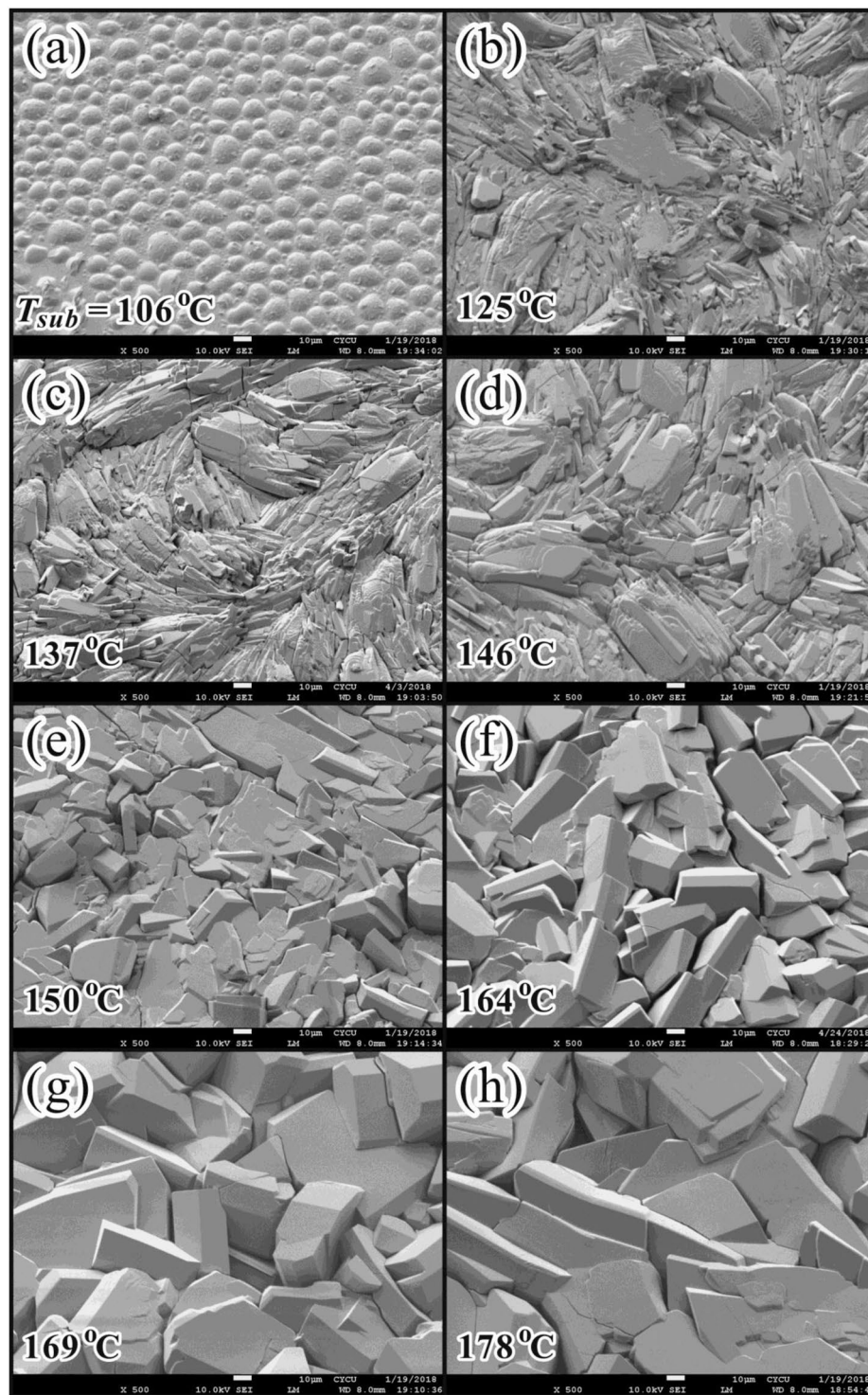


Figure 3. Top-view SEM images on the coumarin-6 polycrystalline films deposited at various T_{sub} with $T_{sou} = 185^\circ\text{C}$.

the coumarin-6 polycrystalline films fabricated at $T_{sub} = 114\sim 178^\circ\text{C}$. This finding indicates that the preferred growth direction of these films on ITO substrate was parallel to the long axis of coumarin-6 molecular crystal. As shown in the inset of Fig. 6(a), the full width at half maximum (FWHM) of these (010) peaks were analyzed by a Gaussian fit with consideration of detector resolution under the same scanning increment. The values of FWHM decreased with increasing T_{sub} for $T_{sub} < 150^\circ\text{C}$ and become saturated for $T_{sub} \geq 150^\circ\text{C}$. The smallest FWHM of $0.027 \pm 0.008^\circ$ (and hence the highest crystallinity of the constituent grains) was obtained for the film deposited at $T_{sub} = 150^\circ\text{C}$. This observation was consistent with the top-view SEM pictures as shown in Fig. 3, where clear facets of crystalline grains emerged in the coumarin-6 films deposited at $T_{sub} \geq 150^\circ\text{C}$.

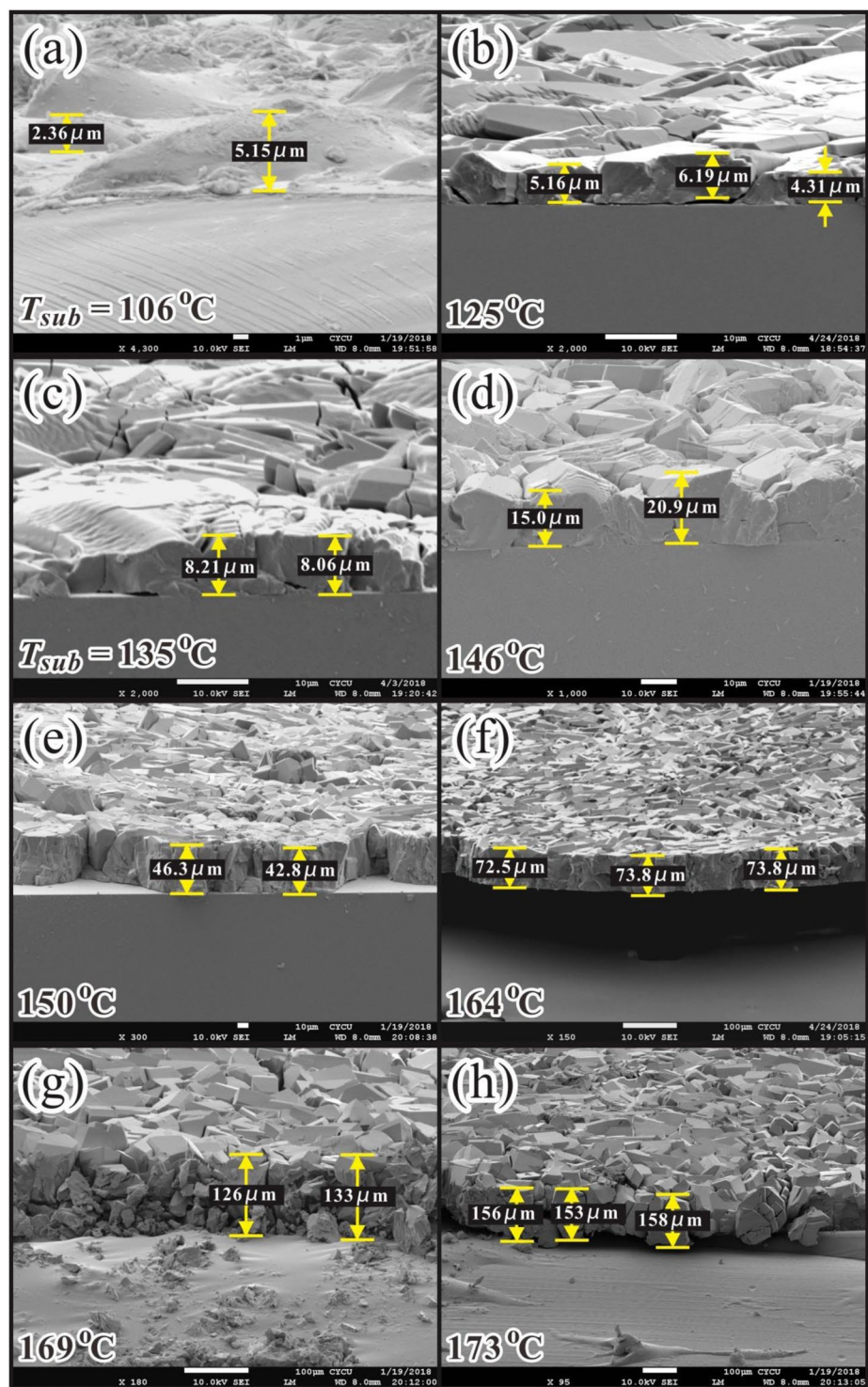
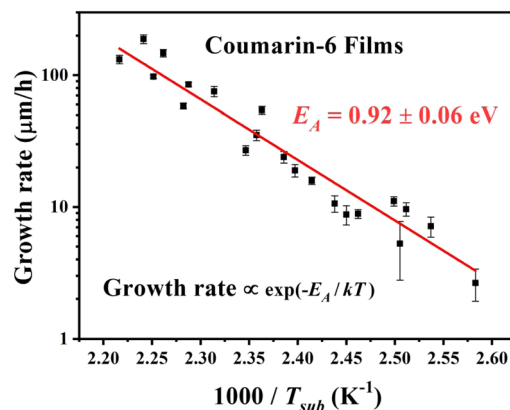


Figure 4. Side-view SEM images on the coumarin-6 polycrystalline films deposited at various T_{sub} with $T_{sou} = 185$ °C. The film thickness is revealed.

Because the intensity of (010) peak was too strong (especially for those coumarin-6 films deposited at $T_{sub} \geq 150$ °C), in linear scale most of the other peaks were suppressed. To reduce the strong (010)-orientation effect from the as-deposited films, the powder-samples were taken from the corresponding films and their XRD results are presented in Fig. 6(b) with logarithmic scale. For a higher T_{sub} (150 or 165 °C, as comparing with 125 °C), the diffraction intensities of the main peaks and of the higher indexed planes were more clearly detected due to the larger surface diffusion energy of the adhered molecules in the growing interface. This finding is consistent with the facts that clear facets were observed for $T_{sub} \geq 150$ °C as shown in Fig. 3. By performing the general structure analysis system (GSAS)²⁷ on these three spectra in Fig. 6(b), the triclinic unit cell volume was estimated



Sample	T_{sou} (°C)	T_{sub} (°C)	E_A (eV)	[Ref.]
C ₆₀	530	260 ~ 435	0.39 ± 0.01	[21]
Alq ₃	280	90 ~ 150	0.54 ± 0.03	[22]
Rubrene	300	103 ~ 221	0.69 ± 0.01	[24]
CuPc	390	140 ~ 320	0.74 ± 0.01	[23]
Coumarin-6	185	114 ~ 178	0.92 ± 0.06	This work

Figure 5. Arrhenius plot of growth rate versus $1000/T_{sub}$ for the coumarin-6 polycrystalline films deposited at various T_{sub} with $T_{sou} = 185^\circ\text{C}$. E_A obtained for some small organic molecular solid films vacuum deposited within the CSS region^{21–24} is summarized.

to be $863.8 \pm 2.1 \text{ \AA}^3$ for $T_{sub} = 125^\circ\text{C}$, $858.8 \pm 0.2 \text{ \AA}^3$ for $T_{sub} = 150^\circ\text{C}$, and $857.3 \pm 0.3 \text{ \AA}^3$ for $T_{sub} = 165^\circ\text{C}$, separately. The packing density of the coumarin-6 molecular crystalline grains became slightly compact for $T_{sub} \geq 150^\circ\text{C}$. The lattice parameters averaged from the grains with high crystallinity fabricated at $T_{sub} = 150$ and 165°C were obtained as followings: $a = 8.965 \pm 0.005 \text{ \AA}$, $b = 11.139 \pm 0.002 \text{ \AA}$, $c = 8.920 \pm 0.007 \text{ \AA}$, $\alpha = 95.13 \pm 0.02^\circ$, $\beta = 104.56 \pm 0.01^\circ$, and $\gamma = 86.72 \pm 0.08^\circ$. These data are in agreement with small crystals growth from supersaturated solutions^{1,14}.

Interestingly, two more peaks at $2\theta \sim 7.410^\circ$ and 9.022° (with a fitted FWHM = 0.126° and 0.075° , correspondingly) in Fig. 6 remain for further discussion. The latter was observable even in linear scale for $T_{sub} < 142^\circ\text{C}$. By using GSAS with zero-check correction, the spacings of parallel planes corresponding to these two peaks were calculated to be $d_1 = 11.89 \pm 0.10 \text{ \AA}$ (which exceeds the longest b -axis length) and $d_2 = 9.77 \pm 0.04 \text{ \AA}$, respectively. To the best of our knowledge, these two peaks have not been reported in the literatures. As mentioned earlier (see Fig. 1), within the coumarin-6 crystalline grains the S- and N-isomers should be distinguished. Due to the random coexistence of the S- and N-isomers within the grains, a reasonable lattice periodicity should be twice or more than the original one. Figure 7 displays the simulated unit cells built in a double-lattice-constant basis from GSAS with isomer-effect consideration. For clarity, only the benzothiazolyl moiety and projection on the ac plane are shown. As illustrated in Fig. 7, the green and red lines characterize two kinds of simulated distances of atom pairs, 11.76 \AA and 9.63 \AA , which closely matched to the experimentally XRD derived spacings of d_1 and d_2 in Fig. 6(b), respectively. Figure 7(a) depicts the crystal structure without isomer-effect consideration, *i.e.*, the projected 2×2 unit cells are identical. The constructive interference cannot be effectively formed by heterogeneous (S and N) atoms in each pair (connected by dotted arrows). However, by exchanging the S and N atoms of the benzothiazolyl moiety in the cells indicated with a light-green background color in Fig. 7(b) to symbolize the exchange between S- and N-isomers, the atoms at both ends of the green and red solid lines become identical. Thus, the constructive interference can be formed by the homogeneous (S or N) atoms in each pair. One final message from Fig. 6(b) is that for $T_{sub} \geq 150^\circ\text{C}$ a weak tail with exponential decay with increasing 2θ after the (010) peak was observed. This phenomenon can be explained in terms of the small interlayer-spacing fluctuations which is commonly detected in two dimensional systems^{28,29}. Thus, the strongly preferred growth direction along (010) plane (which is nearly parallel to the long axis of coumarin-6 molecule as depicted in Fig. 6) might induce a two dimensional characteristics for the coumarin-6 polycrystalline films deposited with $T_{sub} \geq 150^\circ\text{C}$.

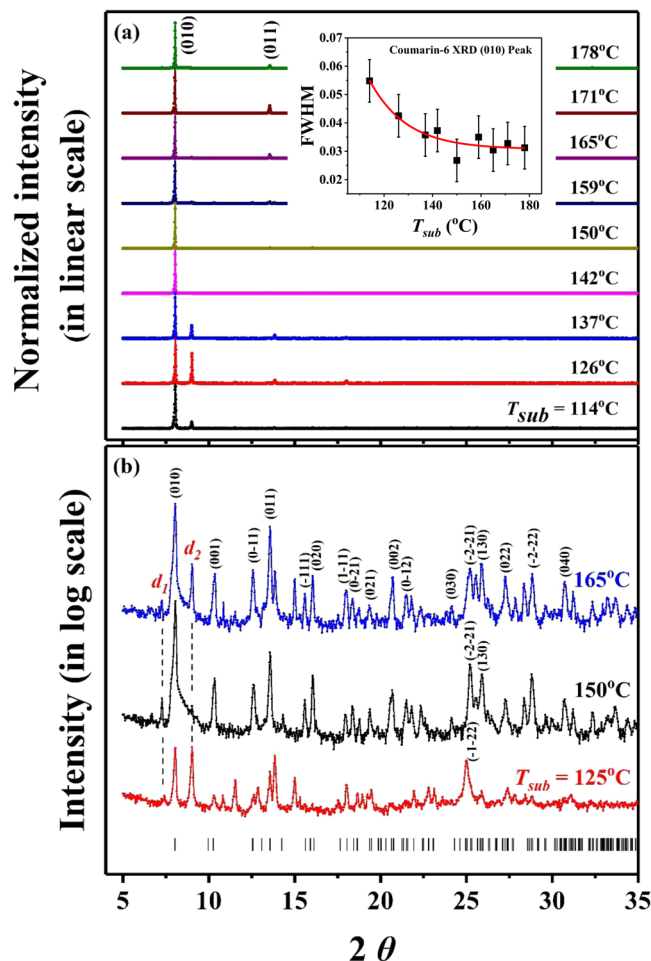


Figure 6. (a) Normalized XRD patterns (in linear scale) on the coumarin-6 polycrystalline films deposited at various T_{sub} with $T_{sou} = 185^\circ\text{C}$. Each curve is shifted up equal distance. The inset shows the variation of FWHM of the (010) peaks with respect to T_{sub} . (b) XRD on the powder-samples taken from the films deposited at $T_{sub} = 125, 150$ and 165°C . The XRD intensities are presented in logarithm scale, and the simulated peak positions from GSAS are shown at the bottom. The Miller indices of the main peaks are assigned based on COD ID 2003249¹.

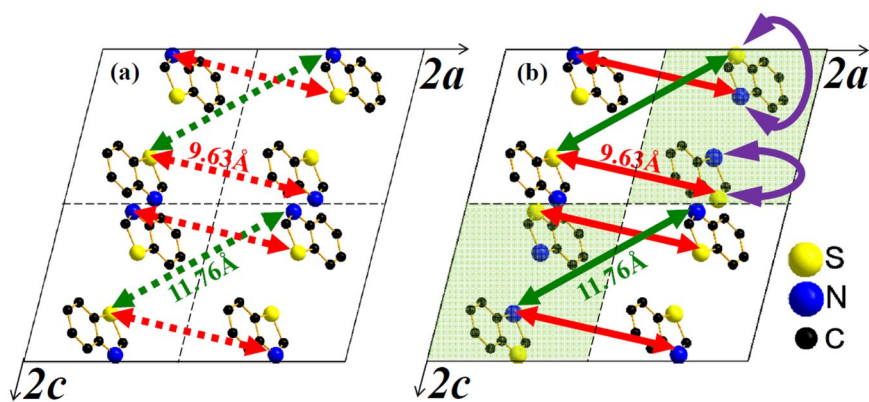


Figure 7. Simulated unit cells built in a double-lattice-constant basis from GSAS. For clarity, only the benzothiazolyl moiety and projection on the ac plane are shown. (a) The projected 2×2 unit cells are identical without isomer-effect consideration. (b) By exchanging the S and N atoms in the benzothiazolyl moiety of the unit cells (indicated with a background of light-green color) to symbolize the change between S- and N-isomers, then the atoms at both ends of the green and red arrows become identical to lead constructive interference peaks as observed in Fig. 6(b).

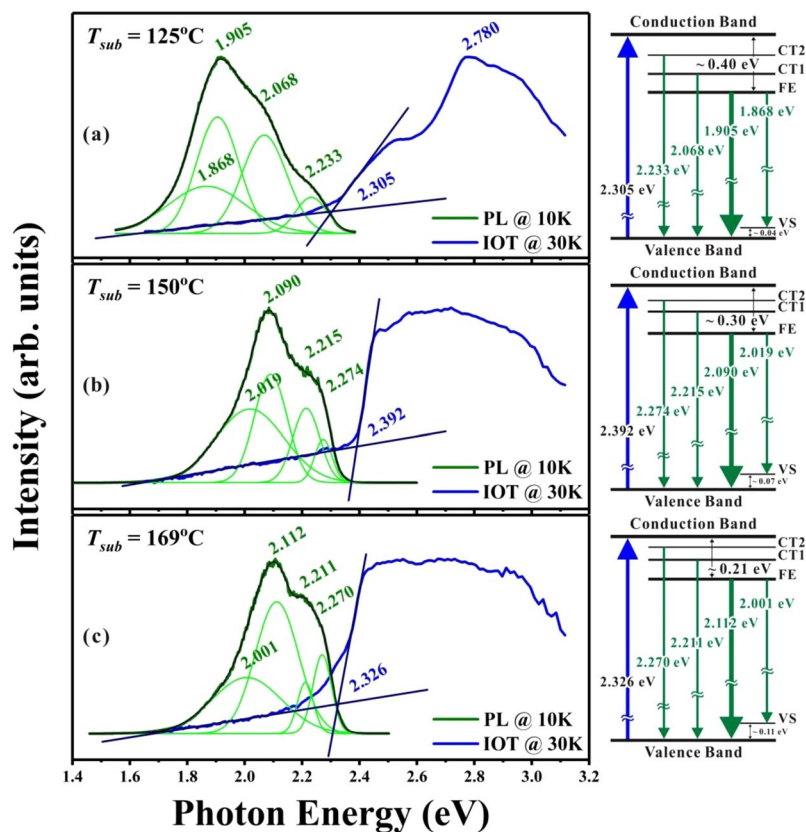


Figure 8. Comparison of the normalized PL and IOT spectra performed at low T for the coumarin-6 polycrystalline films deposited at $T_{sub} =$ (a) 125, (b) 150 and (c) 169 °C with $T_{soli} = 185$ °C. The schematic energy-term diagrams on the right-side summarize the corresponding transitions for E_{op} and for the four PL peaks.

Optical properties of coumarin-6 polycrystalline films. As vaporized small organic molecules condense into an organic molecular solid film, the close pack of splitting electronic levels due to intermolecular interactions forms a continuous electronic band¹⁷. However, in contrast to covalent-bonded inorganic solids, the relatively weak intermolecular interactions in organic molecular solids usually result in a small bandwidth of around 0.5–1.0 eV. Furthermore, the magnitude of optical bandgap (E_{op}) in an organic crystalline solid is expected to be smaller than the energy difference between the lowest unoccupied molecular orbital (LUMO) and the highest occupied molecular orbital (HOMO) of its isolated molecule¹⁷. From the inverse of optical transmission (IOT) spectrum (which is associated with the absorption spectrum), E_{op} can be experimentally deduced. Figure 8 depicts three IOT and PL spectra for coumarin-6 polycrystalline films fabricated with $T_{sub} = 125$, 150, and 169 °C. The absorption threshold (*i.e.*, E_{op}) was practically defined at the intersection of two guide lines²⁵, one for the transmitted background with $h\nu \ll E_{op}$ and the other one for the strong absorption with $h\nu > E_{op}$. For the film deposited at $T_{sub} = 150$ °C, the abrupt increase in IOT spectrum (with smallest band-tail absorption) around E_{op} suggests that this film had a highest crystallinity among other films, and this deduction was consistent with its smallest FWHM detected from Fig. 6(a). Because of its asymmetric molecular structure, coumarin-6 molecules possess a permanent dipole¹⁴, and the strong dipole-dipole interactions may enhance the packing of the adhered molecules. The best crystallinity of coumarin-6 grains observed for $T_{sub} < 150$ °C could be due to a compromise between the increase of the surface diffusion energy for $T_{sub} < 150$ °C and the thermal agitation of the adhered molecules for $T_{sub} > 150$ °C. Thus, the highest $E_{op} = 2.392 \pm 0.007$ eV (with a least band-tail effect) was determined from the coumarin-6 films deposited at $T_{sub} = 150$ °C. Moreover, only for the thin enough films deposited at $T_{sub} \leq 125$ °C, the molecular characters can be revealed in the IOT spectra, and a weak absorption peak around 2.768 ± 0.008 eV was assigned to the HOMO-LUMO transition, which is also consistent with the published results obtained for coumarin-6 molecules dissolved in various solvents⁵.

Complementary to IOT spectra, Fig. 8 compares three normalized PL spectra for coumarin-6 polycrystalline films fabricated at $T_{sub} = 125$, 150, and 169 °C. All the PL spectra can be decomposed into four components by a Gaussian fit with the main peak being assigned to the Frenkel exciton (FE) emission. Accordingly, the weak peak with energy lower than that of FE was attributed to the participation of its molecular vibrational states (VS) because of the rich vibrational motion in coumarin-6 molecule. The other two with energies higher than that of FE were assigned to the charge transfer excitons (CT1 and CT2) in which the electron-hole distances were assigned to the distances between the nearest and next-nearest neighbors of its constituent molecules, respectively. The emergence of CT1 and CT2 might be related to the coexistence of S- and N-isomers within coumarin-6 crystalline grains, which remains for further study. The schematic energy-term diagrams as shown in the right-side of Fig. 8 illustrate

the corresponding transitions for the threshold of absorption (E_{op}) and for the four PL peaks (with the main peak assigned to FE emission). For FE in the molecular solid films, the electron-hole pair is localized on the same molecule¹⁷. Considering the intermolecular interactions, the energy for FE emission and E_{op} in molecular solid films should be different from that in an isolated molecule and are expected to be affected by the packing of its constituent molecules. Hence, as depicted in Fig. 8, E_{op} and the energy positions of PL peaks for coumarin-6 polycrystalline films were varied with T_{sub} , which is consistent with the fact that the unit cell volume simulated by GSAS from the data of Fig. 6(b) were slightly altered with respect to T_{sub} as mentioned above.

Conclusion

Vacuum deposition technique was adopted to deposit coumarin-6 polycrystalline films with T_{sou} determined by a conventional TGA and T_{sub} chosen from a CSS method. Various coumarin-6 films were fabricated with T_{sub} from 106 to 178 °C with a fixed T_{sou} at 185 °C. Because of its slenderness and more asymmetric structure accompanied by a larger permanent dipole, the adhered coumarin-6 molecule on top of the growing interface encounters a higher steric hindrance to occupy the appropriate location and correct orientation, and hence possesses a larger steric energetic barrier of 0.92 eV as estimated from the Arrhenius plot of growth rate versus $1/T_{sub}$. From top-view SEM pictures, for $T_{sub} < 150$ °C, the as-deposited coumarin-6 thin films exhibit a twisted pattern and a kinematic roughness; while for $T_{sub} \geq 150$ °C, clear facets emerge due to the increase of surface diffusion energy. From XRD spectra, a protruding peak assigned to (010) peak reveals that the preferred growth direction of these films on ITO substrate is nearly parallel to the long axis of coumarin-6 molecule. From an analysis of FWHM of the (010) peak, the polycrystalline film deposited at $T_{sub} = 150$ °C exhibits a highest crystallinity among others due to a compromise between surface diffusion and thermal agitation of the adhered molecules. In addition, to account for the two noticeable peaks at $2\theta \sim 9.007^\circ$ and 7.260° , the lattice constants of the triclinic cell should be doubled due to the co-existence of two coumarin-6 isomers, namely, the N-isomer and S-isomer, which are introduced in coumarin-6 crystalline grains for the first time. Furthermore, the bandgap of the coumarin-6 film deposited at $T_{sub} = 150$ °C from OT is estimated to be around 2.392 eV. From PL spectra, four components are obtained by a Gaussian fit. The main peak is assigned to the FE emission; a weak peak with energy lower than that of FE is recognized to the participation of the molecular vibrational states; and the other two with energies higher than that of FE are attributed to charge transfer excitons.

Methods

Fabricating of coumarin polycrystalline films. The vacuum deposition system together with the growth ampoule adopted by this work were described in details in our previous papers^{21–25}. As demonstrated in Fig. 1, an ITO coated glass was chosen as the substrate and adhered underneath a graphite susceptor. A thermocouple was inserted from the other side of the graphite susceptor to monitor T_{sub} *in situ* during the whole process. The temperature profile adopted by T_{sou} was pre-measured by inserting a thermocouple at the bottom of the growth ampoule where the source powder should be located. Due to the different ways of measurement, the steady state temperature profiles adopted for T_{sou} and T_{sub} were slightly shifted as depicted in Fig. 1. Coumarin-6 source powder (with purity > 98.0% from Tokyo Chemical Industry Co., Japan) was used as-received and placed at the bottom of the ampoule. By adjusting the positions of the substrate site relative to the bottom of the ampoule with respect to the temperature profile in a vertical furnace, T_{sou} and T_{sub} could be controlled separately as shown in Fig. 1. After a typical cleaning process, the whole growth ampoule was assembled and loaded with 40–50 mg coumarin-6 source powder, and then kept at room temperature under dynamic vacuum of 5×10^{-2} Torr for 1.0 h to remove residue moisture and vaporized impurities. Next, the growth ampoule was put into a vertical furnace for a preheat process to warm-up the substrate, in which the substrate site was located on a hotter spot with source powder on a colder side for 6–15 min to allow T_{sub} approaching the selected value. After the preheat treatment, the ampoule was pull up to the designated position for vacuum deposition, and it took another 9 ± 1 min for the source powder to reach 95% of the chosen T_{sou} value (in Kelvin temperature scale). The deposition period τ was maintained for 51 ± 1 min under dynamic vacuum condition. At the end of deposition, the growth ampoule was furnace-cooled to room temperature without dynamic vacuum.

Characterization. TGA experiment of coumarin-6 powder was carried out by using a TA Instrument TGA Q50 analyzer under a flow of nitrogen gas with a heating rate of 10 °C/min. The surface morphology as well as the thickness of the as-deposited coumarin-6 polycrystalline film was taken by a JOEL JSM-6335F field emission scanning electron microscopy (SEM). X-ray diffraction (XRD) analysis on coumarin-6 polycrystalline film or powder was performed on a Bruker D8-Advance with Cu-K α emission and with a scanning increment of 0.0149°. Optical transmission (OT) through coumarin-6 film was taken by a scanning monochromator (ARC SpecPro-500) with a tungsten-halogen lamp as the light source. The optical transmittance intensity I_{OT} and the original incident light intensity I_0 were measured by an optometer (Graseby UDT S370) with wavelength correction. Then, the normalized OT spectrum was obtained by dividing I_{OT} by I_0 at each photon energy position. PL spectrum on the coumarin-6 film was performed with exciting by a focused diode laser of 403 nm. The collected luminescence from coumarin-6 film was dispersed by a spectrometer (Jobin Yvon/Spex TRIAX 550) and then detected with a photomultiplier tube. The temperature of the sample site during the OT and PL measurements was controlled by a cryostat system.

References

- Jasinski, J. P. & Paight, E. S. 3-(2-Benzothiazolyl)-7-(diethylamino)-coumarin. *Acta Cryst. C* **51**, 531–533 (1995).
- Edetsberger, M. *et al.* Effective staining of tumor cells by coumarin-6 depends on the stoichiometry of cyclodextrin complex formation. *J. Incl. Phenom. Macrocycl. Chem.* **70**, 327–331 (2011).
- Lakner, P. H. *et al.* Applying phasor approach analysis of multiphoton FLIM measurements to probe the metabolic activity of three-dimensional *in vitro* cell culture models. *Sci. Rep.* **7**, 42730 (2017).

4. Gu, G., Ong, P. P. & Li, Q. Photoluminescence of coumarin 540 dye confined in mesoporous silica. *J. Phys. D: Appl. Phys.* **32**, 2287–2289 (1999).
5. Raikar, U. S. *et al.* Solvent effects on the absorption and fluorescence spectra of coumarins 6 and 7 molecules: Determination of ground and excited state dipole moment. *Spectrochim. Acta A* **65**, 673–677 (2006).
6. Nedumpara, R. J. *et al.* Study of solvent effect in laser emission from coumarin 540 dye solution. *Appl. Optics* **46**, 4786–4792 (2007).
7. Tang, C. W., VanSlyke, S. A. & Chen, C. H. Electroluminescence of doped organic thin films. *J. Appl. Phys.* **65**, 3610–3616 (1989).
8. Hebner, T. R., Wu, C. C., Marcy, D., Lu, M. H. & Sturm, J. C. Ink-jet printing of doped polymers for organic light emitting devices. *Appl. Phys. Lett.* **72**, 519–521 (1998).
9. Jiang, X. *et al.* Doped organic light-emitting diodes based on random copolymers containing both hole and electron transport groups. *Mater. Res. Soc. Symp. Proc.* **558**, 433–438 (2000).
10. Huang, Y.-S., Jou, J.-H., Weng, W.-K. & Liu, J.-M. High-efficiency white organic light-emitting devices with dual doped structure. *Appl. Phys. Lett.* **80**, 2782–2784 (2002).
11. Cheng, J.-A., Chang, C.-P., Chen, C.-H. & Lin, M.-S. The fluorescent quantum efficiency of copolymers containing coumarin-6 at the side-chain. *J. Polym. Res.* **12**, 53–59 (2005).
12. Uddin, A., Lee, C. B. & Wong, J. Emission properties of dopants rubrene and coumarin 6 in Alq₃ films. *J. Lumin.* **131**, 1037–1041 (2011).
13. Lou, Y., Geng, Z., Wang, Z., Naka, S. & Okada, H. Improvement of roll-off in power efficiency for mixed single layer organic light emitting devices by co-doping. *Synth. Metals* **162**, 1204–1209 (2012).
14. Li, X. & Son, Y.-A. C–H···π and C–H···O Interactions in coumarin 6: 3-(2-benzothiazolyl)-7-(diethylamino)-coumarin. *Text. Coloration Finish.* **22**, 83–87 (2010).
15. Laudise, R. A., Kloc, C., Simpkins, P. G. & Sigriest, T. Physical vapor growth of organic semiconductors. *J. Cryst. Growth* **187**, 449–454 (1998).
16. Forrest, S. R. The path to ubiquitous and low-cost organic electronic appliances on plastic. *Nature* **428**, 911–918 (2004).
17. Schwoerer, M. & Wolf, H. C. *Organic Molecular Solids* (Wiley-VCH, Weinheim, Germany, 2005).
18. Price, D. M. & Hawkins, M. Calorimetry of two disperse dyes using thermogravimetry. *Thermochim. Acta* **315**, 19–24 (1998).
19. Price, D. M. Vapor pressure determination by thermogravimetry. *Thermochim. Acta* **367–368**, 253–262 (2001).
20. Chen, R.-S., Lin, Y.-J., Su, Y.-C. & Chiu, K.-C. Surface morphology of C₆₀ polycrystalline films from physical vapor deposition. *Thin Solid Films* **396**, 103–108 (2001).
21. Cheng, W.-R., Tang, S.-J., Su, Y.-C., Lin, Y.-J. & Chiu, K.-C. Effects of substrate temperature on the growth of C₆₀ polycrystalline films by physical vapor deposition. *J. Cryst. Growth* **247**, 401–407 (2003).
22. Jan, D.-J. *et al.* Growth and characterization of tris(8-hydroxyquinoline)-aluminum molecular films. *Thin Solid Films* **520**, 1005–1009 (2011).
23. Chiu, Y.-C., Chen, B.-H., Jan, D.-J., Tang, S.-J. & Chiu, K.-C. Growth behavior of CuPc films by physical vapor deposition. *Cryst. Res. Technol.* **46**, 295–299 (2011).
24. Lin, K.-Y. *et al.* Rubrene polycrystalline films growth from vacuum deposition at various substrate temperatures. *J. Cryst. Growth* **439**, 54–59 (2016).
25. Lin, K.-Y. *et al.* Role of molecular conformations in rubrene polycrystalline films growth from vacuum deposition at various substrate temperatures. *Sci. Rep.* **7**, 408246 (2017).
26. Markov, I. V. *Crystal Growth for Beginners* (World Scientific, Singapore, 1995).
27. Larson, A. C. & von Dreele, R. B. *GSAS General Structure Analysis System* (Los Alamos National Laboratory, New Mexico, USA, 1994).
28. Shi, H., Reimers, J. N. & Dahn, J. R. Structure-refinement program for disordered carbons. *J. Appl. Cryst.* **26**, 827–836 (1993).
29. Zhou, Z., Bouwman, W. G., Schut, H. & Pappas, C. Interpretation of X-ray diffraction patterns of (nuclear) graphite. *Carbon* **69**, 17–24 (2014).

Acknowledgements

The authors gratefully acknowledge financial support from the Ministry of Science and Technology of ROC (Grant numbers MOST 105-2112-M-033-008 and 107-2112-M-033-007).

Author Contributions

K.-L., H.-T. and J.-H. fabricated the samples and performed IOT, SEM and XRD. Y.-S. performed PL. K.-L., Y.-H., C.-C. and K.-C. analyzed XRD data. K.-L., J.-S., J.-L. and K.-C. analyzed IOT and PL spectra. K.-L., C.-C., J.-S., J.-L. and K.-C. contributed through discussion of the manuscript. K.-C. coordinated the study, conducted the project, and wrote the manuscript. All of the authors read and approved the final manuscript.

Additional Information

Competing Interests: The authors declare no competing interests.

Publisher's note: Springer Nature remains neutral with regard to jurisdictional claims in published maps and institutional affiliations.



Open Access This article is licensed under a Creative Commons Attribution 4.0 International License, which permits use, sharing, adaptation, distribution and reproduction in any medium or format, as long as you give appropriate credit to the original author(s) and the source, provide a link to the Creative Commons license, and indicate if changes were made. The images or other third party material in this article are included in the article's Creative Commons license, unless indicated otherwise in a credit line to the material. If material is not included in the article's Creative Commons license and your intended use is not permitted by statutory regulation or exceeds the permitted use, you will need to obtain permission directly from the copyright holder. To view a copy of this license, visit <http://creativecommons.org/licenses/by/4.0/>.

© The Author(s) 2018